Polarized neutron scattering study of the multiple order parameter system NdB_{4}

N. Metoki, H. Yamauchi, M. Matsuda, J. A. Fernandez-Baca, R. Watanuki, and M. Hagihala

Phys. Rev. B **97**, 174416 — Published 17 May 2018

DOI: 10.1103/PhysRevB.97.174416

Polarized Neutron Scattering Study on Multiple Order Parameter System NdB_4

N. Metoki

Materials Sciences Research Center, Japan Atomic Energy Agency, Tokai, Ibaraki 319-1195, Japan and Institute of Quantum Beam Science, Ibaraki University, Tokai, Ibaraki 319-1106, Japan*

H. Yamauchi

Materials Sciences Research Center, Japan Atomic Energy Agency, Tokai, Ibaraki 319-1195, Japan

M. Matsuda and J. A. Fernandez-Baca

Neutron Scattering Division, Oak Ridge National Laboratory, Oak Ridge, Tennessee 37831-6393, USA

R. Watanuki

Faculty of Engineering, Yokohama National University, Yokohama 240-8501, Japan

M. Hagihala

Neutron Scattering Laboratory, Institute for Solid State Physics, University of Tokyo, 5-1-5 Kashiwanoha, Kashiwa, Chiba, 277-8581, Japan

Abstract

Neutron polarization analysis has been carried out in order to clarify the magnetic structures of multiple order parameter f-electron system NdB_4. We confirmed the non-collinear 'all-in all-out' structure (Γ_4) of the in-plane moment, which is in good agreement with our previous neutron powder diffraction study. We found that the magnetic moment along the c-axis m_c showed diagonally antiferromagnetic structure (Γ_{10}), inconsistent with previously reported 'vortex' structure (Γ_2). The microscopic mixture of these two structures with $\vec{q}_0$=$(0,0,0)$ appears in phase II and remains stable in phases III and IV, where an incommensurate modulation coexists. The unusual magnetic ordering is phenomenologically understood via Landau theory with the primary order parameter Γ_4 coupled with higher-order secondary order parameter Γ_{10}. The magnetic moments were estimated to be 1.8 ± 0.2 and $0.2 \pm 0.05\mu_B$ at T=7.5 K for Γ_4 and Γ_{10}, respectively. We also found that a long-period incommensurate modulation of the $\vec{q}_1$=$(0,0,1/2)$ antiferromagnetic structure of m_c with the propagation $\vec{q}_{s1}$=(0.14, 0.14, 0.1) and $\vec{q}_{s2}$=(0.2, 0, 0.1) in phase III and IV, respectively. The amplitude of sinusoidal modulation was about $m_c = 1.0 \pm 0.2\mu_B$ at T=1.5 K. The local $(0,0,1/2)$ structure consists of in-plane ferromagnetic and out-of-plane antiferromagnetic coupling of m_c, opposite to the coexisting Γ_{10}. The m_c of Γ_{10} is significantly enhanced up to $0.6\mu_B$ at T=1.5 K, which is accompanied by the incommensurate modulations. The Landau phenomenological approach indicates the higer-order magnetic and/or multipole interactions based on pseudo-quartet f-electron state play important role.

* metoki.naoto@jaea.go.jp

I. INTRODUCTION

It is becoming ever more apparent that the unusual magnetic properties in rare earth and actinide compounds come from the nature of f-electrons with multiple order parameters and their competing interactions. Multipole ordering has been successfully understood in some light rare-earth [1–5] and actinide [6] compounds with small f-electron number, in most cases $n \leq 2$. The f-electron states and the corresponding excitation spectra under crystalline electric field (CEF) are relatively simple in comparison with heavy rare-earth which are often very complicated and difficult to determine experimentally [7–9].

In this paper, we focused on NdB_4, a challenge for Nd^{3+} with $4f^3$, having $^4I_{9/2}$ ground state. NdB_4 exhibits successive magnetic transitions at $T_0 = 17.2$ K, $T_{N1} = 7.0$ K, and $T_{N2} = 4.8$ K[10]. Previous magnetic and thermodynamic studies revealed the paramagnetic phase I ($T > T_0$), phase II ($T_{N1} < T < T_0$), phase III ($T_{N2} < T < T_{N1}$), and phase IV ($T < T_{N2}$), where the specific heat shows two λ-type anomalies at T_{N1} and T_0, and a first-order-like anomaly at T_{N2}. The system with half-integer J favors magnetic ordering to release the entropy of the Kramers degeneracy.

The mechanism of the successive transitions in NdB_4, especially the type of order parameters, has not been fully understood. The geometrical frustration due to the unique crystal structure [11] with orthogonal dimers of Nd atoms in the Shastry-Sutherland lattice (SS)[12] plays important role; many different type of weak interactions can overcome the frustrating exchange interactions which are usually most dominant, but which are canceled out in NdB_4 due to geometrical effects. It is considered that the successive magnetic transitions are consequence of competition of the order parameters.

Quadrupole ordering coupled with magnetic order parameter is a possible scenario, because the ground state under CEF is a pseudo-quartet, consisting of two Kramers doublets with different orbitals, where the level splitting is comparable to the energy scale of the ordering temperature, namely the strength of the many-body interactions. This pseudo-quartet state, revealed by specific heat measurement and neutron inelastic scattering, carries both the magnetic dipole and electric quadrupole degrees of freedom. The coupling/competing of the magnetic J's and quadrupole O's order parameters could be essential for the unusual physical properties in NdB_4. A similar scenario has been proposed for the iso-structural family DyB_4 and HoB_4.[13–15] In fact, a resonant x-ray study reported the quadrupole ordering

of O_{yz} and O_{zx}, coupled with magnetic order parameters. [14]

The magnetic structures of NdB_4 still remain an open question. Our recent neutron powder diffraction study[11] concluded that the 'all-in all-out' structure (corresponding to the basis vector of Γ_4 irreducible representation[16, 17]) is mixed with a small amount of 'vortex' structure (Γ_2) less than 25% in phase II. Both components with the modulation $\vec{q}_0$=(0, 0, 0) are accompanied by a tetragonal in-plane magnetic moment $m_{\perp c}$. The ordering of only $m_{\perp c}$ is presumed from the result of the magnetic susceptibility; the in-plane susceptibility χ_a shows significant decrease below $T_0 = 17.2$ K, while there is no remarkable anomaly in the out-of-plane susceptibility χ_c at T_0 but Curie-Weiss behavior from high temperatures beyond T_0. This unusual behavior in the magnetic susceptibility was interpreted as the evidence for partial magnetic order[10, 13–15, 18]; the in-plane component of magnetic moment $m_{\perp c}$ is ordered but the c-component m_c remains paramagnetic at $T_0 = 17.2$ K in the case of NdB_4. It means that the magnetic interactions are anisotropic with the in-plane component much stronger than that of out-of-plane. [10] This partial order in NdB_4 should be clarified experimentally.

Note that the behavior of the Γ_2 component is quite unusual; the temperature dependence of the magnetic order parameter is of induced type below the ordering temperature $T_0 = 17.2$ K of main component Γ_4 which is conventional.

Furthermore we were unable to study the low temperature incommensurate phases III and IV. The modulation vectors have been determined as $\vec{q}_{s1} = (0.14, 0.14, 0.1)$ and $\vec{q}_{s2} = (0.2, 0, 0.1)$ in phase III and IV, respectively; $|\vec{q}_{s1}|$ and $|\vec{q}_{s2}|$ are the same but the in-plane orientation is 45° different, namely along the $[1, 1, 0]$ and $[1, 0, 0]$, respectively. These are modulated structures of the antiferromagnetic ordering with $\vec{q}_1 = (0, 0, 1/2)$. The modulation amplitude and its direction should be clarified experimentally. The coexisting commensurate modulation with $\vec{q}_0 = (0, 0, 0)$ in low temperature phases should also be studied. The steep decrease in χ_c at T_{N1} suggests the order of m_c below T_{N1}, thus the commensurate structure may be different from phase II. Especially in phase IV, the relative intensities of magnetic reflections for $\vec{q}_0$ are significantly different from the ones for phase II.

For our purpose, neutron polarization analysis (NPA) is one of the most powerful methods. This technique provides the spin-dependent neutron scattering cross section which is sensitive to the phase and the direction of the magnetic moment, by controlling the scattering vector $\vec{Q}$ and the direction of the neutron spin with respect to the crystal orientation

as well as the neutron spin state. Therefore it is highly powerful to identify and decompose the basis vectors predicted from the magnetic group theory; they are often characterized by the moment direction even if their extinction rules are similar. We succeeded in obtaining a complete picture of the magnetic structures in NdB_4. It also demonstrates the powerfulness of NPA using a high quality single crystal.

II. EXPERIMENT

High quality NdB_4 single crystal samples were grown by the floating zone method in a four-ellipsoidal mirror-type image furnace. The ^{11}B isotope enriched to 99.5% was used in order to prevent neutron from strong absorption. Two rectangular-shaped samples with dimensions of typically $4\times2\times2$ mm^3 were prepared. The sample was fixed on an Al sample holder with H-free glue, and lapped with thin Al foil. We measured three different crystal orientations with changing two samples alternatively to minimize the beam time loss. The sample was cooled down to 1.5 K using a standard liquid-He cryostat.

NPA has been carried out using the triple-axis spectrometer (PTAX) installed at HB-1 beam port of HFIR in ORNL, USA. The neutron beam with the incident energy of 13.5 meV was monochromatized and polarized using Heusler(111) monochrometer/analyzer crystals. The flipping ratio more than 17 for nuclear scattering guarantees the high reliability of the present NPA The data, after correction of this finite flipping ratio are presented in this paper. The incident neutron spin (+) can be flipped (−) by Mezei-type, flipper located between the monochrometer and sample, while only neutrons with spin up (+) were analyzed and counted by a ^{3}He detector. The guide field was applied either parallel to the scattering vector $\vec{Q}$ (HF) or vertical to the (horizontal) scattering plane (VF). Thus all four scattering cross sections in HF-SF, HF-NSF, VF-SF, and VF-NSF channels can be measured, here SF and NSF indicate the spin-flip $(-+)$ and non-spin-flip $(++)$ cross sections, obtained by flipper ON or OFF, respectively. HF-NSF channel provides the nuclear scattering, while HF-SF includes the total magnetic scattering of the moment perpendicular to the scattering vector $\vec{Q}$. On the other hand, VF-NSF contains scattering from the vertical magnetic moment interfered with the nuclear scattering, whereas VF-SF is given only by the magnetic moment in the horizontal scattering plane and also perpendicular to $\vec{Q}$. Nuclear spin polarization can be ignored in the temperature range of this study. NPA is powerful because of this

TABLE I. Magnetic moment which contributes to the scattering intensity of polarization channels with $(H, K, 0)$, $(H, 0, L)$, and (H, H, L) scattering planes. The subscript *ver.* and *hor.* indicate vertical and horizontal components, while b denotes nuclear scattering.

	HF-NSF	HF-SF	VF-NSF	VF-SF
$(H, K, 0)$			$b\,, m_c$	$m_{\perp c}$
$(H, 0, L)$	b	$m_c\,, m_{\perp c}$	$b\,, (m_{\perp c})_{ver.}$	$m_c, (m_{\perp c})_{hor.}$
(H, H, L)			$b\,, (m_{\perp c})_{ver.}$	$m_c, (m_{\perp c})_{hor.}$

sensitivity to the moment direction, a definitive probe to identify and decompose the basis vector having a certain moment orientation. In our case three scattering planes of $(H, K, 0)$, (H, H, L), and $(H, 0, L)$ are measured; the c-axis is vertical and horizontal in the first and last two orientation geometries, respectively. In the $(H, K, 0)$ scattering geometry we can unambiguously determine m_c and $m_{\perp c}$ by VF-NSF and VF-SF, separately. The (H, H, L) and $(H, 0, L)$ orientations were measured to study the incommensurate modulation of phase III and phase IV, respectively. The direction of the modulation amplitude can be determined with quantitative intensity calculations; in these scattering geometries m_c is only observed in VF-SF, while the horizontal and vertical components of $m_{\perp c}$ provide signals in VF-SF and VF-NSF, respectively. Clearly, the observation of VF-NSF indicates the existence of $m_{\perp c}$. Note that we can expect both horizontal and vertical components of $m_{\perp c}$ from the in-plane tetragonal symmetry, when $m_{\perp c}$ exists. The interference term of nuclear and magnetic scattering in VF-NSF can be ignored, because the guide field is too small to obtain a single-domain antiferromagnetic structure. The observed components for various scattering geometries are summarized in Table I.

III. RESULTS

We now describe the results in the following three subsections for the structures with $\vec{q}_0$, $\vec{q}_{s1}$, and $\vec{q}_{s2}$ modulations. Note that $\vec{q}_0$ modulation exists in all three magnetic phases II, III, and IV, while $\vec{q}_{s1}$ and $\vec{q}_{s2}$, coexisting with $\vec{q}_0$, appears only in phase III and IV, respectively. Our previous paper concluded the magnetic structure of $\vec{q}_0$ modulation in phase II is the

ordering of main component Γ_4 characterized by the very strong $(1,1,0)$ reflection, coexisting with weakly induced component Γ_2 accompanying very weak $(1,0,0)$ reflection, respectively. Thus NPA of these characteristic reflections was carried out very carefully in order to reveal $m_{\perp c}$, accompanied by the basis vector of the irreducible representations Γ_4 and Γ_2.

A. $\vec{q}_0$ modulation

The scattering profiles of $(1,1,0)$ reflection measured with the rocking curve on the (H,K,0) scattering plane are shown in Fig. 1(a) at T= 1.5 K, (b) T= 6.0 K, (c) T= 7.5 K, and (d) T= 20 K in phase IV, III, II, and I (paramagnetic phase) of NdB_4, respectively. We observed that the data measured in HF-SF channel is the same as for VF-SF, where both of them are of magnetic origin. No difference in these two SF cross sections is the evidence for the magnetic moment in the horizontal scattering plane, namely $m_{\perp c}$. It is also consistent with the no difference in VF-NSF from HF-NSF channel which is the total nuclear scattering. No contribution of magnetic scattering in VF-NSF channel involves the ordered moment $m_{\perp c}$. These are consistent with our recent neutron powder diffraction study which has been concluded Γ_4 as the main component of $\vec{q}_0$ modulation in phase II.

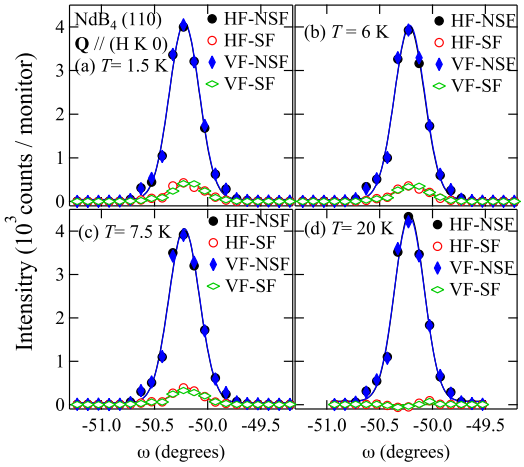

FIG. 1. (Color online) Spin polarized neutron scattering profile of the $(1,1,0)$ refection of NdB_4 measured at (a) $T = 1.5$ K in phase IV, (b) $T = 6.0$ K in phase III, (c) $T = 7.5$ K in phase II, and (d) $T = 20$ K in the paramagnetic phase I.

Figure 2 shows the rocking curves of the $(1,0,0)$ reflection for (a) T= 1.5 K , (b) T= 6.0 K, and (c) T= 7.5 K in phase IV, III, and II of NdB_4, respectively. In all three phases, we observed a remarkable peak in HF-SF but no signal in HF-NSF, indicating that the $(1,0,0)$ reflection is of purely magnetic origin. We also confirmed the absence of the $(1,0,0)$ reflection in the paramagnetic phase I; the flat intensity at the peak position was at background level. Furthermore the peak observed in VF-NSF is the same as HF-SF, while no trace of VF-SF. It means that the $(1,0,0)$ reflection comes from the scattering by the magnetic moment along the vertical c-axis, namely m_c which is not expected from Γ_2 as shown in Fig. 5 in Ref. [11]. Therefore our previous model for the magnetic structure in phase II was inconsistent with this experimental result. Note that no $(1,0,0)$ reflection is expected from the calculation of magnetic structure factor for Γ_4. This means that the $(1,0,0)$ reflection can be attributed to a minor component of the magnetic order parameter with m_c.

The intensities of the $(1,1,0)$ and $(1,0,0)$ reflections are shown as a function of temperature in Fig. 3(a) and (b), respectively. The $(1,1,0)$ intensity in VF-SF channel increases

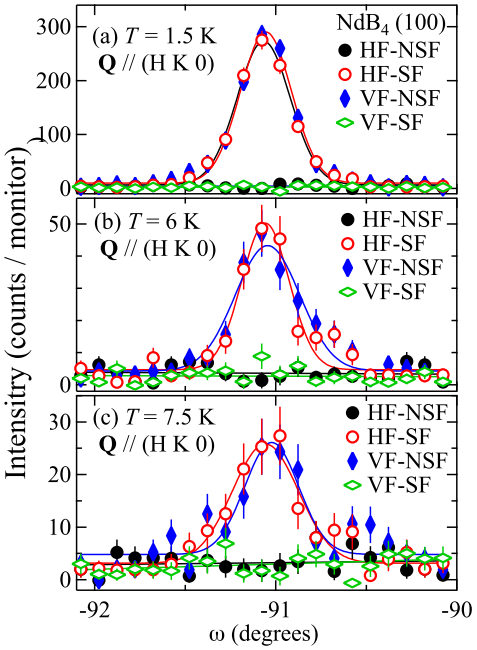

FIG. 2. (Color online) Spin polarized neutron scattering profile of the $(1,0,0)$ refection of NdB_4 measured at (a) T = 1.5 K in phase IV, (b) T = 6.0 K in phase III, and (c) T = 7.5 K in phase II, respectively.

continuously below $T_0 = 17.2$ K, exhibiting the growing magnetic order parameter with $m_{\perp c}$ of the irreducible representation Γ_4. The temperature dependence of the Γ_4 order parameter is quite smooth beyond the phase boundaries at $T_{\rm N1} = 7.0$ K and $T_{\rm N2} = 4.8$ K down to T= 1.5 K; no characteristic change associated with the ordering at $T_{\rm N1}$ and $T_{\rm N2}$ can be recognized. Thus Γ_4 is stable in the whole temperature range of phases II, III, and IV.

There is a very small deviation of the HF-SF intensity from the VF-SF intensity of the $(1, 1, 0)$ reflection below $T < 12$ K, more clearly below $T_{\rm N2} = 4.8$ K as shown in Fig. 3(a). This small difference is the contribution from the minor component of the magnetic order parameter with m_c as observed in $(1, 0, 0)$ reflection. A very small deviation of the VF-NSF intensity from the HF-NSF intensity below $T < 2$ K in Fig. 3(a) would have the same origin. This deviation is more difficult to detect due to the large nuclear background, requiring very good statistics. Note that this small contribution was not detected in the data of Fig. 1, because of the larger statistical error and shorter counting time compared to those for Fig. 3(a). We simply point out that these contributions from the minor components of the magnetic order parameter with m_c are quantitatively consistent with the intensity

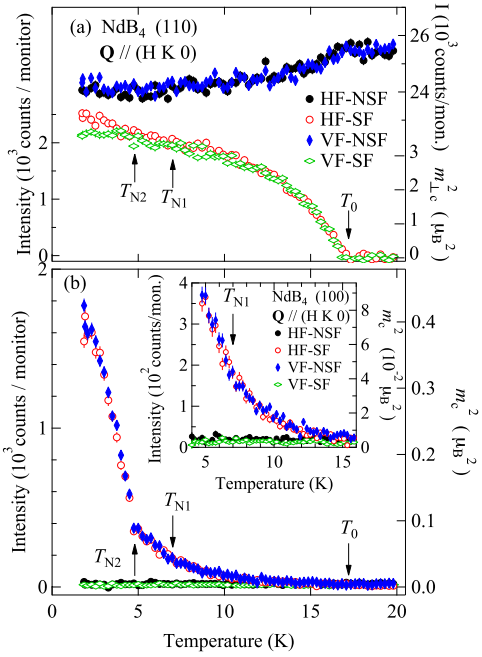

FIG. 3. (Color online) The temperature dependence of the scattering intensities of (a) $(1, 1, 0)$ and (b) $(1, 0, 0)$ reflections, respectively. The inset has an expanded scale.

calculations based on the experimentally determined magnetic structure Γ_{10} accompanying m_c described below.

The HF-NSF and VF-NSF intensities of the $(1,1,0)$ reflection are almost constant in the observed temperature range; a small decrease below $T_0 = 17.2$ K may come from a dynamical or multiple scattering effect for the high-quality single crystal sample. A small structural change can not be ruled out from the present experimental data. This possibility should be checked by X-ray scattering technique using synchrotron radiation.

The temperature dependences of the $(1,0,0)$ scattering intensities for the four spin dependent cross sections are shown in Fig. 3(b). The $(1,0,0)$ intensities in HF-SF and VF-NSF channels are very small in the vicinity of $T_0 = 17.2$ K, while they show gradual increase with a clear concave curvature with decreasing temperature. The intensities change continuously but the slope increases slightly at $T_{\rm N1} = 7.0$ K; the temperature dependence may be linear for $T_{\rm N2} < T < T_{\rm N1}$ or weakly convex. The intensities increase steeply below $T_{\rm N2} = 4.8$ K. Since the HF-NSF intensity is at the background level determined by the intensity for $T > T_0$, the $(1,0,0)$ reflection is purely magnetic origin, while no intensity in VF-SF as well as no difference between HF-SF and VF-NSF intensities are the evidence for the magnetic order parameter with m_c.

The ordered moment $m_{\perp c}$ of Γ_4 structure can be estimated from the magnetic structure factor of VF-SF compared with nuclear scattering observed in HF-NSF channel, which is great advantage using NPA. The obtained is shown on the right-hand axis for VF-SF channel in Fig. 3(a). Note that only the $m_{\perp c}$ component of Γ_4 contributes to VF-SF channel. On the other hand, m_c was obtained by NPA of the (2,1,0) reflection, and also calculated from the (1,0,0) reflection intensity after the structural analysis relevant to the irreducible representation of Γ_{10} induced order parameter. We obtained $m_c = 0.2 \pm 0.05 \mu_{\rm B}$ and $m_{\perp c} = 1.8 \pm 0.2 \mu_{\rm B}$, corresponding to the net moment $1.8 \pm 0.2 \mu_{\rm B}$ at $T_{\rm N1}$. With decreasing temperature down to $T = 1.5$ K, $m_{\perp c}$ is almost flat and increases up to $m_{\perp c} = 1.9 \pm 0.2 \mu_{\rm B}$, while m_c shows steep increase up to $m_c = 0.6 \pm 0.1 \mu_{\rm B}$. The net moment and the $m_{\perp c}$ of Γ_4 at $T = 7.5$ K are consistent with our previous study[11] within the experimental accuracy.

These temperature dependences are fully consistent with our recent unpolarized neutron scattering experiment (See Fig. 4 in ref. [11]). The unusual temperature dependence of $(1,0,0)$ in the temperature range of phase II indicates that this component is of induced-type. It is clear that the magnetic interactions in NdB_4 is anisotropic; the magnetic interaction

for the in-plane component is much larger than that for out-of-plane component. The anisotropic interaction can be understood from the difference in the transition temperatures $T_0 = 17.2$ K and $T_{\rm N1} = 7.0$ K, where $m_{\perp c}$ and m_c show critical behavior, respectively. A small critical field of the magnetization about 3 T along the c-axis is also the evidence for weak interaction of the c-component.[10] Therefore, it is reasonable to conclude that a small m_c is induced as the secondary order parameter by $m_{\perp c}$ in phase II.

From Landau theory, critical behavior of only single component of irreducible representation, Γ_4 in this case, is a necessary condition for the second-order transition. We believe Landau criteria are maintained at T_0, because m_c is infinitesimally smaller than $m_{\perp c}$ at the critical point T_0; m_c is a higher-order secondary order parameter. It can be demonstrated by the tilt angle ϕ of the Nd moment from the tetragonal ab-plane, calculated with the equation,

$$\phi = \tan^{-1} \frac{m_c}{m_{\perp c}}, \tag{1}$$

assuming both m_c and $m_{\perp c}$ on the same site. The temperature dependence of angle ϕ in Fig. 4 shows a gradual increase from $\phi = 0$ in the vicinity of T_0, indicative of critical behavior of single component of irreducible representation Γ_4.

Figure 5(a) shows the integrated intensities which are proportional to $(m_{\perp c})^2$, obtained

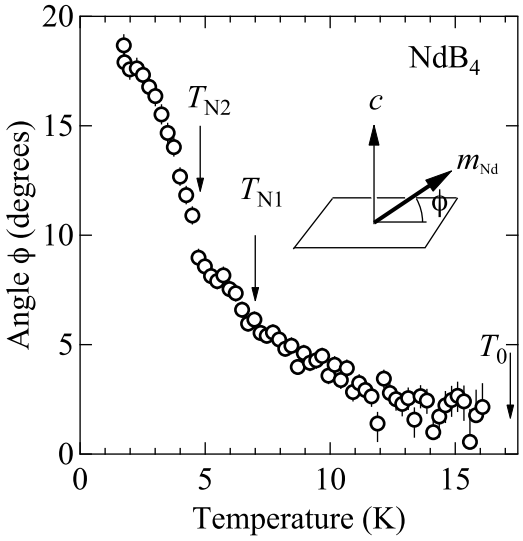

FIG. 4. The angle ϕ of the Nd moment from the tetragonal c-plane as a function of temperature. The angle ϕ is schematically denoted in the inset.

from VF-SF channel. The $(m_{\perp c})^2$ can also be estimated from the data in the other channels, I(HF-SF)−I(VF-NSF)+I(HF-NSF). The consistency was confirmed for each reflection. The data in the ordered phases II ($T = 7.5$ K), III ($T = 6$ K), and IV ($T = 1.5$ K), denoted by open squares, open circles, and close triangles in Fig. 5(a), respectively, are very similar and consistent with the model calculation for Γ_4 structure.

After the component of the ordered moment has been identified, we can analyze scattering intensity data using the magnetic scattering cross section given as,

$$\left(\frac{d\sigma}{d\Omega}\right)_{el} = \frac{1}{N_m}\frac{(2\pi)^3}{v_0}\sum_{\vec{\mathbf{G}}_\mathbf{M}} \delta\left(\vec{Q} - \vec{\mathbf{G}}_\mathbf{M}\right)\left|\vec{\mathbf{M}}_\perp\left(\vec{Q}\right)\right|^2, \tag{2a}$$

$$\vec{\mathbf{M}}\left(\vec{Q}\right) = \gamma r_0 \sum_j^{unit\ cell} f_j\left(\vec{Q}\right)\vec{m}_j \exp\left[i\vec{Q}\cdot\vec{r}_j - W_j\left(\vec{Q}\right)\right], \tag{2b}$$

$$\vec{\mathbf{M}}_\perp\left(\vec{Q}\right) = \hat{\mathbf{Q}} \times \vec{\mathbf{M}}\left(\vec{Q}\right) \times \hat{\mathbf{Q}}\,, \tag{2c}$$

here, N_m and v_0 are the number and the volume of the magnetic unit cell, $\vec{\mathbf{G}}_\mathbf{M}$ is the magnetic reciprocal vector, m_j is the magnetic moment of the j^{th} atom at $\vec{r}_j$ with the Debye-Waller factor W_j. γ, r_0, and f are the gyromagnetic ratio, classical electron radius, and magnetic form factor, respectively. Equation (2c) gives the projection $\vec{\mathbf{M}}_\perp$ of the magnetic structure factor $\vec{\mathbf{M}}$ onto the plane perpendicular to the scattering vector $\vec{Q}$, where $\hat{\mathbf{Q}}$ is the unit vector parallel to $\vec{Q}$. The calculation of $\vec{\mathbf{M}}_\perp$ is very easy in the present case; the contribution of m_c which is perpendicular to $\vec{Q}$ for $(H, K, 0)$ scattering plane is separated from $m_{\perp c}$ using NPA. The present result is in good agreement with our recent neutron powder diffraction study.[11] Similar non-collinear structures have been reported in U_2T_2X with the same space group $P4/mbm$ and magnetic U atoms at $4h$[19, 20]; Nd at $4g$ site has the same site symmetry shifted 1/2 along z.

Figure 5(b) shows the integrated intensity of some representative reflections with $\vec{q}_0 = (0, 0, 0)$ measured on the $(H, K, 0)$ scattering plane. The intensities in VF-NSF subtracted by HF-NSF and also HF-SF subtracted by VF-SF, are proportional to $(m_c)^2$. Note that the interference term of the nuclear and magnetic scattering in VF-NSF channel vanishes due to the antiferromagnetic domain structure.

The intensity in the HF-SF channel is given by $\vec{\mathbf{M}}_\perp$ composed of m_c and $m_{\perp c}$. The

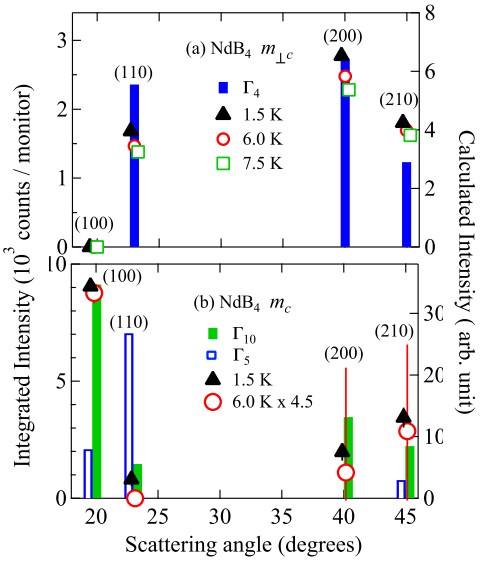

FIG. 5. (Color online) The integrated intensities of the magnetic scattering from (a) $m_{\perp c}$ and (b) m_c obtained from neutron polarization analysis. The data denoted by symbols are compared with the model calculation for the basis vector of the irreducible representations (a) Γ_4, (b) Γ_5 and Γ_{10} indicated by bars. Solid lines are statistical errors.

relative intensities observed at $T = 1.5$ K (phase IV) and 6 K (phase III) denoted by close triangles and open circles in Fig. 5(b), respectively, are very similar. At $T = 7.5$ K in phase II a weak but clear signal of $(1, 0, 0)$ reflection was observed, while those for $(1, 1, 0)$, $(2, 0, 0)$, and $(2, 1, 0)$ reflections were too weak to detect within the statistical error. Thus the relative intensities relevant to m_c is very similar in phase II. The magnetic structure with m_c is identical and stable in the ordered phases II, III, and IV.

We can propose three possible candidates for the magnetic structure with m_c, which are Γ_3, Γ_5, and Γ_{10}, given by the basis vector of the irreducible representations of NdB_4; the magnetic moments at Nd $4g$ site in the space group $P4/mbm$ with $q_0 = (0, 0, 0)$. These magnetic structures are schematically shown in Fig. 6. By comparing the data with model calculation using Eq. (2a), we found only Γ_{10} can explain the present experimental result with very strong $(1, 0, 0)$ and very weak $(1, 1, 0)$, while Γ_5 is opposite. The characteristic feature in Γ_{10} is the antiferromagnetic coupling/interaction of m_c's along the diagonal direction in

a chemical unit cell. This is in good agreement with the picture of SS lattice composed of frustrated antiferromagnetic dimers.[12] Consequently the coupling of m_c's along the a-axis is ferromagnetic but antiferromagnetic along b which is crystallographically equivalent to a (Γ_{10}-1), and vice versa (Γ_{10}-2). They form iso-energetic domains of two-dimensional representation Γ_{10}. On the other hand, m_c of Γ_5 couple ferromagnetically along the diagonal direction, implying no frustration due to ferromagnetic dimer. Γ_3, the ferromagnetic order of m_c, can be immediately ruled out from the absence of the ferromagnetic moment in previous susceptibility and magnetization measurements on NdB_4.

The magnetic structure in phase II is shown in Fig. 7, which is described as a combination of irreducible representations Γ_4 and Γ_{10}.

We may have a question, the magnetic structure is composed of whether the macroscopic coexistence or microscopic mixing of magnetic order parameters Γ_4 and Γ_{10}. Our scattering experiments cannot distinguish these two possibilities, but we conclude a microscopic mixture from the temperature dependences of m_c and $m_{\perp c}$. The magnetic moment m_c as large as $1.7\mu_B$ has been reported in a recent study under the magnetic field H >3.5 T along the c-axis. The macroscopic mixture is equivalent to the inhomogeneity with two phase coexistence in a sample; some region is Γ_4 and the other is Γ_{10}. In this case, the scattering

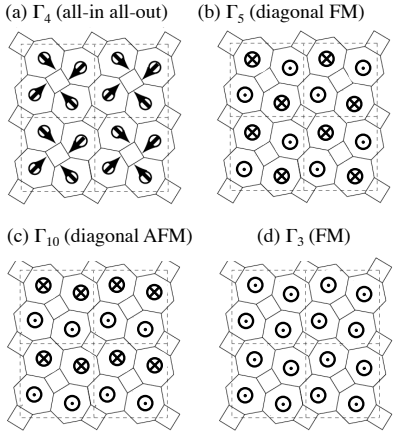

FIG. 6. The magnetic strictures described by the basis vector of the irreducible representations (a) Γ_4, (b) Γ_5, (c) Γ_{10}, and (d) Γ_3, respectively. Broken lines indicate the unit cell. Solid circles with dots denote the Nd moments 'up', while solid circles with crosses mean 'down'.

intensity is proportional to the volume fraction of these phases. Thus, a steep increase of $(1,0,0)$ intensity below $T_{\rm N2} = 4.8$ K indicates the growing volume fraction of Γ_{10} up to roughly 30% at the expense of the same volume of Γ_4, which should result in a steep decrease of the $(1,1,0)$ intensity below $T_{\rm N2}$. Obviously it is not the case, because the $(1,1,0)$ intensity shows a flat temperature dependence below $T_{\rm N2}$ as in Fig. 3(a). The in-plane ordered moment remains $m_{\perp c} = 1.9\mu_{\rm B}$, which corresponds to the saturation magnetization of Nd. A local probe like NMR gives helpful information to distinguish macroscopic two phase coexistence or microscopic mixture of the order parameters.

The $(1,0,0)$ reflection was also observed in the $(H,0,L)$ scattering geometry, in which m_c is lying in the horizontal scattering plane. We obtained consistent results with the experiment of $(H,K,0)$ scattering geometry mentioned above. However strong contaminations of nuclear multiple scattering were superposed in HF-NSF and VF-NSF channels even in the paramagnetic phase. The intensities in these two channels were the same, and showed no temperature dependence. Therefore, we concluded that these were multiple scattering contaminations, and magnetic intensities were not included in the VF-NSF channel. The magnetic signal was clearly observed in the HF-SF channel and the same intensity as in VF-SF. These mean the magnetic moment parallel to the horizontal c-axis, only m_c, contributes to the $(1,0,0)$ refection.

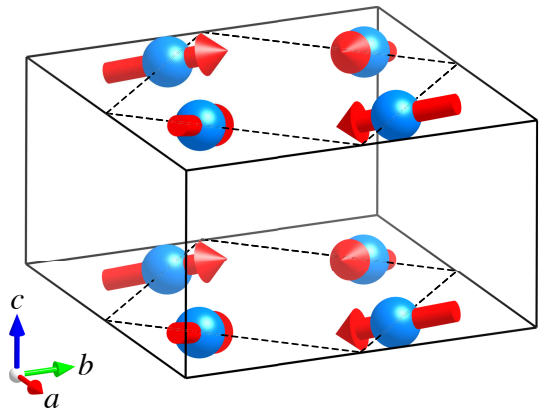

FIG. 7. (Color online) The magnetic structure of phase II.

B. $\vec{q}_{s2}$ modulation in phase IV

Neutron polarization analysis was carried out with the $(H, 0, L)$ scattering geometry at $T = 1.5$ K in order to observe the magnetic reflections coming from the modulation vector $\vec{q}_{s2} = (0.2, 0, 0.1)$ and its equivalents. Here, note that the c-axis lies in the horizontal scattering plane. Figure 8 shows the representative profiles of the H- and L-scan for $(-0.2, 0, 0.4)$, $(-1.8, 0, 0.4)$ and $(-1.8, 0, 1.6)$ reflections. We observed clear magnetic satellite peaks at $(H,0,L + 0.5)\pm\vec{q}_{s2}$, where H and L are integers. No trace of scattering intensity was recognized in HF-NSF channel, indicating no nuclear contribution at the incommensurate positions. The incommensurate structure is a long-period modulation of the $\vec{q}_1$=$(0, 0, 1/2)$ antiferromagnetic structure. This $(0, 0, 1/2)$ antiferromagnetic structure can be described with the one dimensional antiferromagnetic stacking along the c-axis, $+ - +-$, where $+$ or

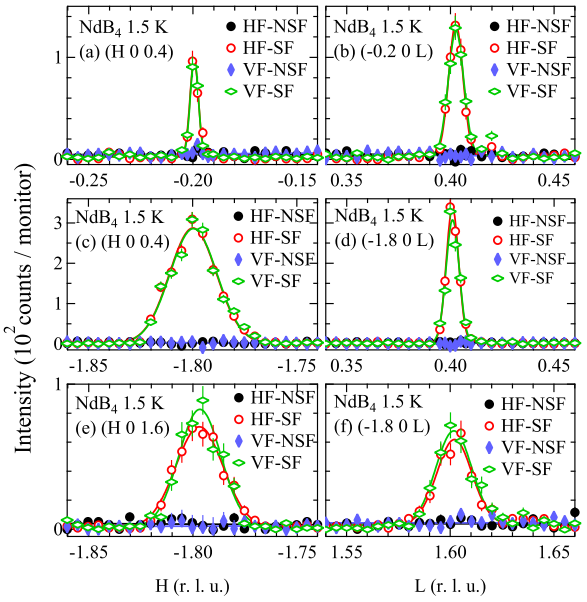

FIG. 8. (Color online) Spin polarized neutron scattering profile of the incommensurate peak with $\vec{q}_{s2} = (0.2, 0, 0.1)$ measured at $T = 1.5$K in phase IV. The upper, middle, and lower panels indicate $(-0.2, 0, 0.4)$, $(-1.8, 0, 0.4)$, and $(-1.8, 0, 1.6)$ reflections, respectively. The left- and right-hand side panels show H- and L-scan, respectively.

− indicate ferromagnetically ordered ab-plane. The direction of the modulation amplitude is considered to be parallel to the c-axis. In Fig. 8 the magnetic scattering is observed in HF-SF and VF-SF channels with the same intensity. Therefore the ordered moment is in the horizontal scattering plane, most likely only m_c. $m_{\perp c}$ could contribute SF channels, when it has a component in the horizontal scattering plane. However we expect $m_{\perp c}$ both in horizontal and vertical direction because of the tetragonal symmetry of NdB_4. Therefore the absence of the magnetic scattering in VF-NSF channel strongly suggests the modulation amplitude along the c-axis. Furthermore, the scattering intensity of $(-1.8, 0, 0.4)$ is much stronger than those for $(-0.2, 0, 0.4)$ and $(-1.8, 0, 1.6)$ reflections. The intensity is strong, when the scattering vector $\vec{Q}$ is close to be perpendicular to the c-axis. From the angle factor of the magnetic scattering, it suggests that m_c contributes the magnetic scattering.

The successive magnetic transition from the phase III to IV is of the first order. Therefore, we could not apply the representation analysis, requiring the condition 'the second order transition from a paramagnetic phase'. Instead, we tried to explain our experimental results, assuming simple structures shown in Fig. 6(b)-(d) modulated with $\vec{q}_{s2}$. The absence of a peak for H close to 1, for example, no (0.86 , 0 , 0.4) peak can be reproduced by the calculation of magnetic structure factor based on Fig. 6(d).

Figure 9 shows the normalized integrated intensities of various magnetic satellite peaks

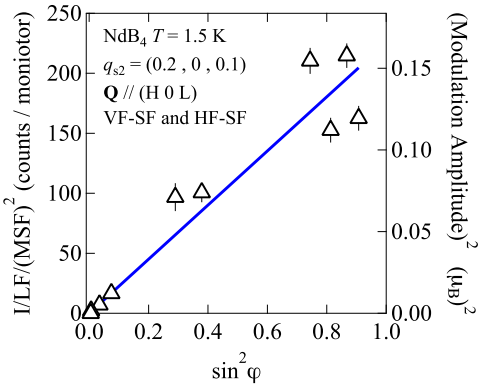

FIG. 9. (Color online) The integrated intensities of the incommensurate peaks with the modulation $\vec{q}_{s2}$ measured at $T = 1.5$ K. The intensities are normalized with Lorentz factor and squared magnetic structure factor (including magnetic form factor) and plotted as a function of $\sin^2\varphi$, where φ is the angle between the c-axis and $\vec{Q}$

obtained from HF-SF and VF-SF plotted as a function of $\sin^2\varphi$, where φ is the angle between the c-axis and the scattering vector $\vec{Q}$. The scattering cross section for the satellite reflections of the sinusoidal modulation can be given using Eq. (2a) as

$$\left(\frac{d\sigma}{d\Omega}\right) = \frac{1}{2}\frac{(2\pi)^3}{N_m v_0}\sum\left|\vec{\mathbf{M}}_\perp\left(\vec{\mathbf{G}}_\mathbf{M}\right)\right|^2 \delta\left(\vec{\mathbf{Q}} - \vec{\mathbf{G}}_\mathbf{M} \pm \vec{q}\right). \tag{3}$$

When one-dimensional modulation of m_c is assumed, we get,

$$\vec{\mathbf{M}}_\perp\left(\vec{\mathbf{G}}_\mathbf{M}\right) = \vec{\mathbf{M}}\left(\vec{\mathbf{G}}_\mathbf{M}\right)\sin\varphi. \tag{4}$$

Therefore the intensity should be proportional to $\sin^2\varphi$ when it is normalized by the Lorentz factor and squared magnetic structure factor (including magnetic form factor for the Nd^{3+} ion), which is recognized in Fig. 9. It means that the modulation amplitude is parallel to the c-axis, namely m_c. The size of the modulation amplitude is also shown on the right hand side axis in Fig. 9. We obtained that the modulation amplitude is about $1.0 \pm 0.2\mu_\mathrm{B}$ at $T = 1.5$ K.

C. $\vec{q}_{s1}$ modulation in phase III

The magnetic structure with the long-period modulation $\vec{q}_{\mathrm{s}1}$ was also studied at $T = 6$ K in a similar manner but on (H, H, L) scattering plane to observe the the incommensurate satellite reflections. We obtained similar results as those for $\vec{q}_{\mathrm{s}2}$. Figure 10(a) shows the result of $(0.14, 0.14, 0.4)$ reflection. We observe a clear peak with HF-SF and VF-SF channels with no difference, while the HF-NSF and VF-NSF channels are in the background level. The incommensurate modulation along the c-direction can be recognized from the L-scan in Fig. 10(b) which shows the scattering peak measured with VF-SF channel. These results can be interpreted as well as those for $\vec{q}_{\mathrm{s}2}$ modulation; the modulation amplitude is expected to be parallel to the c-axis, namely m_c. We have also confirmed the direction of the modulation from the integrated intensities which is proportional to $\sin^2\varphi$ as shown in Fig. 11. Here we assumed the modulation of the FM structure with $\vec{q}_{\mathrm{s}1}$. Representation analysis is not applicable, because the phase III emerges from the magnetically ordered phase II. The large scattering of the data in Fig. 11 is due to very weak intensity and limited beam time for

polarization set up. The size of the modulation amplitude was estimated as $0.4 \pm 0.1 \mu_{\rm B}$ at $T = 6$ K. This tiny moment from a small sample and with large neutron absorption due to ^{10}B contamination made NPA very difficult.

IV. DISCUSSION

In our previous study[11], the possibility of the irreducible representations with m_c were rejected from the candidate of the induced order parameter. It came from a simple argument of 'partial ordering' hypothesis which assumed a paramagnetic state remaining along the c-axis, thus $m_c = 0$ in phase II. According to our present study, we have to point out that an induced higher-order moment can exist statically, even when the susceptibility remains paramagnetic-like. The unusual behavior of the magnetic susceptibility can be attributed to the complicated character of f-electron states with a large orbital moment, which strongly depends on the CEF and the variety of interactions including multipole degrees of freedom for (pseudo) degenerated states. We need the information of f-electron states treated with appropriate interactions in order to understand the unusual behavior of NdB_4 in microscopic manner.

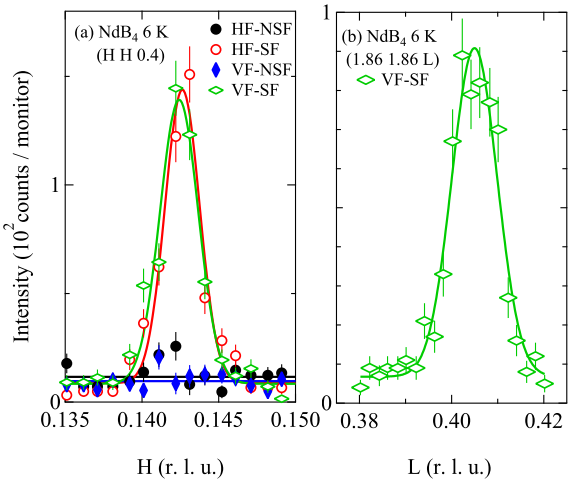

FIG. 10. (Color online) Spin polarized neutron scattering profile of the incommensurate peak with $\vec{q}_{\rm s1} = (0.14, 0.14, 0.1)$ measured at $T = 6$ K in phase III. (a) $(H, H, 0.4)$ and (b) $(1.86, 1.86, L)$ scan.

The successive ordering of the tetragonal c-moment and in-plane moment is reminiscent of previous studies on $NpTGa_5$ (T: Fe, Ni, and Rh,).[21–24] Mean-field calculations [25, 26] predict the quadrupole ordering of O_{xy} and O_{zx} coupled with $J_{x,y}$ and J_z in the pseudo-triplet ground state. Therefore, this type of successive transition would be a general phenomenon, independent of the number of f electrons, whether $4f$ or $5f$, Kramers (NdB_4 and DyB_4) or non-Kramers (HoB_4 and $NpTGa_5$). We believe a similar scenario can explain the successive transition in NdB_4. A development of this scenario would be necessary to explain the unusual behavior of a small induced moment m_c in microscopic manner.

We tried to analyze our neutron powder diffraction data published before based on the correct model with $\Gamma_4 + \Gamma_{10}$ revealed by this NPA study. Consequently the neutron powder diffraction data were fitted as well as our previous analysis with a wrong model based on $\Gamma_4 + \Gamma_2$; no significant improvement of the reliability factors was recognized. It was very hard to distinguish these two models without very high quality powder diffraction data. This study clearly demonstrates the powerfulness of NPA on a single crystal coupled with group theoretical analysis, and how risky to determine the magnetic structure only from powder diffraction data.

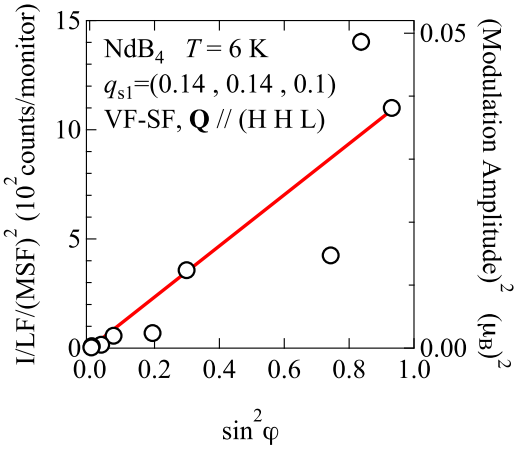

FIG. 11. (Color online) The integrated intensities of the incommensurate peaks with the modulation $\vec{q}_{s1}$ measured at $T = 6$ K. The intensities are normalized with Lorentz factor and squared magnetic structure factor (including magnetic form factor) and plotted as a function of $\sin^2\varphi$, where φ is the angle between the c-axis and $\vec{Q}$

It is not easy to explain the small m_c in phase II from the anisotropic magnetic interactions. The 90° coupling of Nd moment (Γ_4) may come from higher-order biquadratic interactions. Exchange interactions are cancelled out because of the geometrical frustration. The m_c modifies this Γ_4 structure against the 90° coupling. The local FM structure of m_c exhibits critical behavior in phase III. The transition temperature $T_{\rm N1} < T_0$ is indicative of the weak FM interaction for m_c. Furthermore, this FM interaction cannot contribute to induce the m_c with AFM (Γ_{10}) structure in phase II. A simple and plausible scenario is the coupling of the order parameters: the m_c is induced by $m_{\perp c}$, mediated by the coupling with O_{yz} and O_{zx}. Both the m_c (Γ_{10}) and $m_{\perp c}$ (Γ_4) are diagonally AFM. This coherence can be reasonably understood with the coupling model. Then, the order parameters can be analyzed with Landau theory, including the coupling term of order parameters.

The unusual behavior of the magnetic ordering in NdB_4 can be phenomenologically understood based on Landau theory without the information of f-electron state. The free energy $\mathcal{F}_0$ can be expressed by a polynomial of the order parameter ψ,

$$\mathcal{F}_0 = \alpha\,(T - T_{\rm c})\,\psi^2 + \beta\,\psi^4, \tag{5}$$

where $\alpha, \beta > 0$ are coefficients for the 2^{nd} and 4^{th} order term, respectively. The derivative $\partial\mathcal{F}_0/\partial\psi = 0$ gives ψ which minimizes $\mathcal{F}_0$;

$$\mathcal{F}_0 = 0 \text{ at } \psi = 0 \ \ (\text{for } T > T_{\rm c})\,, \tag{6a}$$

$$\mathcal{F}_0 = -\beta\,\psi^4 \text{ at } \psi = \pm\sqrt{\frac{\alpha}{2\beta}\,(T_{\rm c} - T)} \ \ (\text{for } T \le T_{\rm c})\,. \tag{6b}$$

The first term in Eq.(5) becomes negative below the critical temperature $T < T_{\rm c}$, yielding a double minimum of $\mathcal{F}_0$ at a finite ψ given in Eq. (6b). This framework can be extended to the system with the secondary order parameter ξ which is induced by ψ.[6] The free energy expansion $\mathcal{F}_2$ is the polynomials of ξ with the same order of ψ in Eq. (5). ξ is given as the higher-order order parameter with n^{th} power ψ^n.

$$\mathcal{F} = \mathcal{F}_0 + \mathcal{F}_2, \tag{7}$$

$$\mathcal{F}_2 = -\delta\,\psi^{2n}\xi^2 + \epsilon\,\xi^4. \tag{8}$$

In the first term of $\mathcal{F}_2$, ψ is included instead of $(T - T_c)$ as a coefficient of ξ^2. Thus a finite ξ is induced with $\psi \neq 0$, associated with the phase transition at the single critical point T_c. ξ is obtained by minimizing $\mathcal{F}_2$ with the derivative $\partial\mathcal{F}_2/\partial\xi = 0$, analogous to the case for ψ,

$$\mathcal{F}_2 = 0 \text{ at } \xi = 0 \ \ (\text{for } T > T_c)\,. \tag{9a}$$

$$\mathcal{F}_2 = -\epsilon\,\xi^4 \text{ at } \xi = \pm\sqrt{\frac{\delta}{2\epsilon}}\psi^n \ \ (\text{for } T \leq T_c)\,. \tag{9b}$$

Equation (9b) indicates that ξ is order of ψ^n.

The primary order parameter is not affected by the presence of the secondary order parameter, when $\mathcal{F}_2$, namely the coefficients δ and ϵ, are negligibly small in comparison with $\mathcal{F}_0$. In higher-order case with $n \geq 2$, $\mathcal{F}_2$ is less important in the critical region, $1 \gg \psi \gtrsim 0$ for $T \lesssim T_c$.

This framework of the Landau theory can be applied to NdB_4, where we consider ψ as the primary order parameter of Γ_4, and ξ as the induced secondary order parameter of Γ_{10} representations, respectively. Obviously $n = 1$ is not allowed for NdB_4 from the Landau criteria for the second order transition at T_0, because ψ and ξ belong to the different irreducible representations of Γ_4 and Γ_{10}. A linear combination ($n = 1$) of ψ and ξ belonging to the same irreducible representation could exhibit critical behavior of both of them, as the coupled primary order parameter.

Figure 12 shows the plot of the magnetic intensities observed by VF-NSF channel of the $(1, 0, 0)$ reflection as a function of those obtained from VF-SF of the $(1, 1, 0)$ reflection. These are the same data as in Fig. 3 which shows the temperature dependences of the intensities of these reflections. The magnetic intensities for $(1, 0, 0)$ and $(1, 1, 0)$ are proportional to $(m_c)^2$ and $(m_{\perp c})^2$, respectively, i.e., order parameter squared. Thus the data in Fig. 12 can be analyzed with the following equation,

$$\xi^2 \propto \left(\psi^2\right)^n. \tag{10}$$

As shown in Fig. 12 and the inset with the logarithmic scale after subtracting the background, we can recognize n would be in the range of 3 to 6, suggesting the higher-order magnetic or multipole coupling.

No influence of the secondary order parameter on the primary one is also consistent with the present experimental results concerning the stability of Γ_4 below T_0 with no remarkable change at $T_{\rm N1}$ and $T_{\rm N2}$, where the m_c exhibits significant increase.

It is really a surprising result that the structure of m_c in Γ_{10} is completely different from those for the two incommensurate modulations. The m_c in Γ_{10} is antiferromagnetic along the in-plane diagonal direction, while the incommensurate modulations show locally ferromagnetic alignment of m_c in the tetragonal c-plane, which is coupled antiferromagnetically along the c-axis. This can be understood from the long-period incommensurate modulation of the $\vec{q}_1 = (0, 0, 1/2)$ antiferromagnetic structure with the modulation vectors $\vec{q}_{\rm s1}$ and $\vec{q}_{\rm s2}$ and their equivalents.

The second order transition at $T_{\rm N1}$ is also unusual, because m_c is already non-zero above $T_{\rm N1}$. However, this is allowed, because the order parameter is the Fourier component of

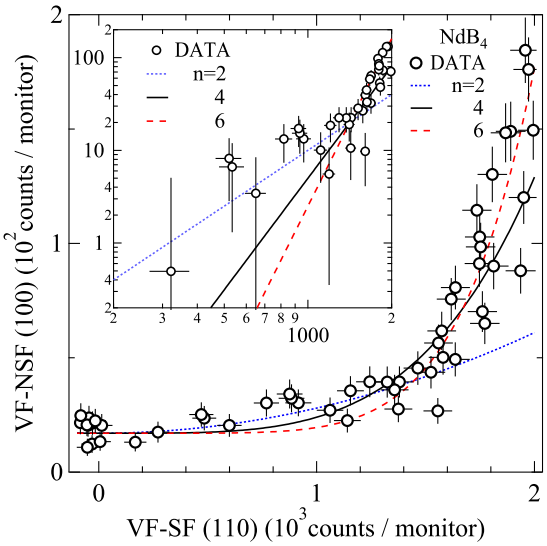

FIG. 12. (Color online) Plot of the $(1, 0, 0)$ magnetic scattering intensity measured with VF-NSF channel as a function of the $(1, 1, 0)$ magnetic scattering intensity measured with VF-SF channel, which are attributed to m_c^2 and $m_{\perp c}^2$, respectively. The inset is the logarithmic plot.

m_c with $\vec{q}_{s1}$. The non-zero m_c with $\vec{q}_0$ (Γ_{10}) can be coupled with the short-range correlation/fluctuation with $\vec{q}_{s1}$. The intensity of (1,0,0) reflection increases steeply below 10 K as shown in Fig. 3(b). This mode coupling is the origin of the long tail of the specific heat up to 10 K.[10]. When the temperature is close to T_{N1}, the correlation length increases and thus, the $\vec{q}_{s1}$ mode is decoupled from the m_c with $\vec{q}_0$. The second order transition emerges at T_{N1}, where the correlation grows up to infinite.

The existence of the lock-in transition at T_{N2} may suggest the complex Fermi surface topology mediating RKKY interactions in a complicated (or competing) manner, which is coupled with the magnetic as well as multipole degrees of freedom of f-electrons in NdB_4. It may be related to the intensity of $(1, 0, 0)$ reflection increasing steeply in phase IV, but not significantly in phase III.

V. CONCLUSION

The magnetic structures of NdB_4 were determined by means of NPA. In phase II they are composed of $\vec{q}_0 = (0, 0, 0)$ structures described by the basis vectors of irreducible representations for Γ_4 and Γ_{10}. There are long-period modulations of the $\vec{q}_1 = (0, 0, 1/2)$ antiferromagnetic structure of m_c with $\vec{q}_{s1} = (0.14, 0.14, 0.1)$ or $\vec{q}_{s2} = (0.2, 0, 0.1)$ in phase III and phase IV, respectively, coexisting with $\vec{q}_0$ modulation. The magnetic moments at T=1.5 K were estimated to be $m_{\perp c} = 1.9 \pm 0.2\mu_B$ and $m_c = 0.6 \pm 0.1\mu_B$ for Γ_4 and Γ_{10}, respectively, while the incommensurate modulation amplitude was $m_c = 1.0 \pm 0.2\mu_B$. Landau theory provides a phenomenological picture of the coupled order parameters, but the f-electron state and the multipole interactions should be revealed for the microscopic understanding of the unusual behavior of NdB_4.

ACKNOWLEDGMENTS

We thank Prof. R. Robinson for the stimulating discussion. The neutron scattering experiment at Oak Ridge National Laboratory was supported by the U.S.–Japan Cooperative Program on Neutron Scattering. Research conducted at ORNL's High Flux Isotope Reactor was sponsored by the Scientific User Facilities Division, Office of Basic Energy Sciences, US Department of Energy. This work was supported by a Grant-in-Aid for Scientific Research

(C) (No. 25390133) from the Japan Society for the Promotion of Science.

---

[1] T. Matsumura, T. Yonemura, K. Kunimori, M. Sera, and F. Iga, Phys. Rev. Lett. **103**, 017203 (2009), and references there in.

[2] M.Kohgi, K.Iwasa, M.Nakajima, N.Metoki, S.Araki, N.Bernhoeft, J.-M.Mignot, A.Gukasov, H.Sato, Y.Aoki and H.Sugawara, J. Phys. Soc. Jpn. **72**, 1002 (2003).

[3] K. Kaneko, N. Metoki, R. Shiina, T. D. Matsuda, M. Kohgi, K. Kuwahara, and N. Bernhoeft, Phys. Rev. **B 75**, 094408 (2007).

[4] K. Kuramoto, H. Kusunose, and A. Kiss, J. Phys. Soc. Jpn. **B 78**, 072001 (2009).

[5] T. Onimaru and H. Kusunose, J. Phys. Soc. Jpn. **B 85**, 082002 (2016).

[6] P. Santini, S. Carretta, G. Amoretti, R. Caciuffo, N. Magnani, and G. H. Lander, Rev. Mod. Phys. **81**, 807 (2009).

[7] H. Yamauchi, H. Onodera, K. Ohoyama, T. Onimaru, M. Kosaka, M. Ohashi, and Y. Yamaguchi, J. Phys. Soc. Jpn. **68**, 2057 (1999).

[8] Y. Tanaka, T. Inami, T. Nakamura, H. Yamauchi, H. Onodera, K. Ohoyama, and Y. Yamaguchi, J. Phys.: Condens. Matter **11**, L505 (1999).

[9] K. Hirota, N. Oumi, T. Matsumura, H. Nakao, Y. Wakabayashi, Y. Murakami, and Y. Endoh, Phys. Rev. Lett. **84**, 2706 (2000).

[10] R. Watanuki, T. Kobayashi, R. Noguchi, and K. Suzuki, J. Phys.: Conf. Ser. **150**, 042229 (2009)

[11] H. Yamauchi, N. Metoki, R. Watanuki, K. Suzuki, H. Fukazawa, S. Chi, and J. A. Fernandez-Baca, J. Phys. Soc. Jpn. **86**, 044705 (2017).

[12] B. S. Shastry and B. Sutherland, Physica **B 108**, 1069 (1981).

[13] D. Okuyama, T. Matsumura, H. Nakao, and Y. Murakami, J. Phys. Soc. Jpn. **74**, 2434 (2005).

[14] T. Matsumura, D. Okuyama, T. Mouri, and Y. Murakami, J. Phys. Soc. Jpn. **80**, 074701 (2011).

[15] D. Okuyama, T. Matsumura, T. Mouri, N. Ishikawa, K. Ohoyama, H. Hiraka, H. Nakao, K. Iwasa, and Y. Murakami, J. Phys. Soc. Jpn. **77**, 044709 (2008).

[16] A. S. Wills, Physica **B 276-278**, 680 (2000).

[17] A. S. Wills, Phys. Rev. **B 63**, 064430 (2001).

[18] R. Watanuki, G. Sato, K. Suzuki, M. Ishihara, T. Yanagisawa, Y. Nemoto, and T. Goto, J. Phys. Soc. Jpn. **74**, 2169 (2005).

[19] A. Purwanto, R. A. Robinson, L. Havela, V. Sechovský, P. Svoboda, H. Nakotte, K. Prokeš, F. R. de Boer, A. Seret, J. M. Winand, J. Rebizant, and J. C. Spirlet, Phys. Rev. **B 50**, 6792 (1994).

[20] H. Nakotte, A. Purwanto, R. A. Robinson, K. Prokeš, J. C. P. Klaasse, P. F. de Châtel, and F. R. de Boer, L. Havela and V. Sechovský, L. C. J. Pereira, A. Seret, J. Rebizant, and J. C. Spirlet, F. Trouw, Phys. Rev. **B 53**, 3263 (1996).

[21] N. Metoki, J. Phys. Soc. Jpn. **75** [Suppl.], 24 (2006).

[22] S. Jonen, N. Metoki, F. Honda, K. Kaneko, E. Yamamoto, Y. Haga, D. Aoki, Y. Homma, Y. Shiokawa, and Y. Ōnuki, Phys. Rev. **B 74**, 144412 (2006).

[23] F. Honda, N. Metoki, K. Kaneko, S. Jonen, E. Yamamoto, D. Aoki, Y. Homma, Y. Haga, Y. Shiokawa, and Y. Ōnuki, Phys. Rev. **B 74**, 144413 (2006).

[24] S. Kambe, H. Sakai, Y. Tokunaga, R. E. Walstedt, D. Aoki, Y. Homma, and Y. Shiokawa, Phys. Rev. **B 76**, 144433 (2007).

[25] A. Kiss and Y. Kuramoto, J. Phys. Soc. Jpn. **75**, 034709 (2006).

[26] A. Kiss and Y. Kuramoto, J. Phys. Soc. Jpn. **77**, 124708 (2008).